Coherent transfer matrix analysis of the transmission spectra of Rydberg excitons in cuprous oxide

Heinrich Stolz,[1,*] Rico Schwartz,[1] Julian Heckötter,[2] Marc Aßmann,[2] Dirk Semkat,[3] Sjard O. Krüger,[1] and Manfred Bayer[2]

[1]*Institut für Physik, Universität Rostock, Albert-Einstein-Straße 23-24, 18059 Rostock, Germany*

[2]*Experimentelle Physik 2, Technische Universität Dortmund, 44221 Dortmund, Germany*

[3]*Institut für Physik, Ernst-Moritz-Arndt-Universität Greifswald, Felix-Hausdorff-Straße 6, 17489 Greifswald, Germany*

(Received 19 September 2020; accepted 29 June 2021; published 23 July 2021)

In this paper, we analyze the transmission spectrum of a thin plate of cuprous oxide in the range of the absorption of the yellow exciton states with the coherent transfer matrix method. We demonstrate that, in contrast to the usual analysis using the Bouguer-Lambert law, a consistent quantitative description over the whole spectral range under consideration is possible. This leads to more accurate parameters not only for the Rydberg exciton states but also for the strengths of indirect transitions. Furthermore, the results have consequences for the interaction of Rydberg excitons with other systems, e.g., Rydberg states themselves or for the determination of the density of electron-hole pairs after optical excitation.

DOI: 10.1103/PhysRevB.104.035206

I. INTRODUCTION

The recent experimental observation of excitons with high quantum numbers up to $n = 25$ in cuprous oxide Cu_2O at low temperatures [1] has triggered a series of papers on the behavior of these Rydberg excitons in electric and magnetic fields, as maser materials, for studies of quantum properties of matter, etc. (for an overview, see Ref. [2]). On the other hand, we expect that, due to their fragile character, Rydberg excitons are extremely sensitive probes for every kind of deviation from a perfect crystal, so that the presence of other excitations in the crystal, e.g., a plasma of electron-hole pairs, will influence the absorption lines. Indeed, as has been found recently, the presence of an electron-hole plasma or uncompensated impurities with densities around 10^{10} cm^{-3} already quenches the absorption of P states with high quantum numbers ($n > 20$) [3–6].

These Rydberg excitons are usually detected as resonances in the transmission spectrum of a thin sample. For details of the experimental setup, see Refs. [1,2]. In the analysis of the transmission spectra, one hitherto assumed [1,2] that multiple reflections and interferences at the sample surfaces can be neglected due to the high absorption. Then one can convert a measured transmission $T(\lambda_{\text{probe}})$ into the absorption coefficient $\alpha(E)$ by the simplified expression based on Bouguer-Lambert's law [7,8]:

$$\alpha(E) = -\frac{\ln\left(C_{\text{refl}} C_{\text{streu}} T\right)}{d} = -\frac{\ln\left[\frac{T(\lambda_{\text{probe}})}{T_0}\right]}{d}, \qquad (1)$$

where C_{refl} and C_{scat} are the reflection and scattering losses at the window and sample surfaces, d is the thickness of the sample, and $E = 2\pi\hbar c_0/\lambda_{\text{probe}}$ is the photon energy ($\hbar$ is Planck's constant, and c_0 the velocity of light in vacuum). Also, the use of the optical density $\alpha(E)d$ is common [1,2]. Since the scattering losses are not well known, one usually looks for a spectral region where, due to physical reasons (e.g., in a semiconductor well below the lowest exciton transitions), the absorption coefficient is zero. Then one can take T_0 as the measured transmission in this region. In the spectrum shown in Fig. 1, this has been done by starting the measurement well below the yellow $1S$ ortho exciton quadrupole transition (marked by *). For a very thin sample also, the thickness is not well known. From mechanical measurements, we estimate for our sample $d_{Cu_2O} = (33 \pm 3)\ \mu$m, but one can determine it more accurately by adjusting the absorption coefficient to the well-known value around the Γ_3^- absorption edge (at $E_{1Sy,\Gamma_3^-} = 2.046165$ eV [9]) given by [10]

$$\alpha(E) = \alpha_0\sqrt{E - E_{1Sy,\Gamma_3^-}}\ \text{meV}^{-1/2}; \quad \alpha_0 = (8 \pm 0.25)\ \text{cm}^{-1}. \qquad (2)$$

The dependence of α for higher photon energies is also well known [11,12], so that the indirect absorption coefficient can be continued. Furthermore, it is well known [13] that the absorption lines of the yellow P states are sitting on top of this phonon background. Since both processes lead to the same final state, we observe for the P lines an asymmetric Lorentzian line shape.

The result for the indirect absorption background is shown by the dashed blue lines in Fig. 1. Obviously, there is no agreement between the measured and calculated absorption coefficient around the P lines. The absorption coefficient from Eq. (1) is smaller than that expected from the indirect process. On first sight, this means that the determination of T_0 is not correct. However, an additional absorption band around the indirect absorption threshold must have a very peculiar line shape (it must exactly compensate for the square root behavior around the threshold) and would also require a much smaller

*heinrich.stolz@uni-rostock.de

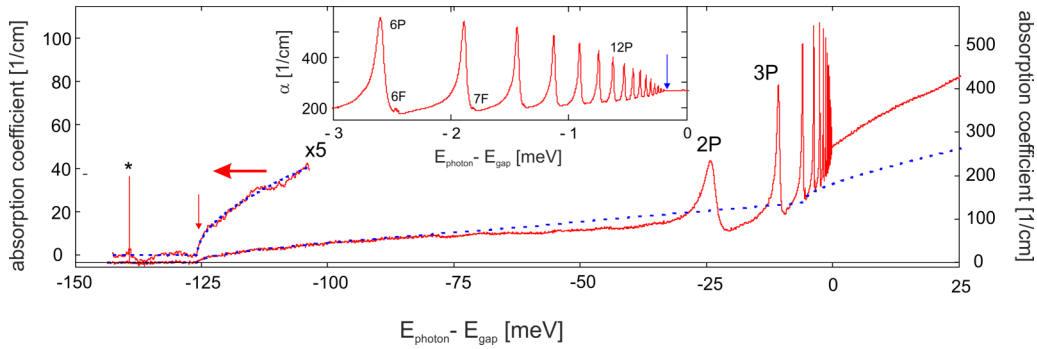

FIG. 1. Experimental results for absorption coefficient of Cu_2O [calculated with Eq. (1)] from the transmission spectrum (red line) plotted vs the difference of photon energy and band gap from the yellow $1S$ ortho quadrupole transition (marked by *) to beyond the band gap of the yellow exciton (zero of the abscissa). The left side shows the spectrum around the indirect band gap with enlarged scale (×5). The blue lines are the calculated phonon-assisted absorption. The red vertical arrow indicates the indirect Γ_3^- absorption edge. The inset shows the absorption below the band gap with P lines up to $n = 22$. The blue vertical arrow denotes the apparent gap position.

sample thickness. Changing the value of α_0 in Eq. (2) is not possible, as it is an intrinsic property of Cu_2O. Therefore, a highly likely other reason that might lead to such a behavior is an interference effect. Its occurrence seems to be quite possible due to the long coherence length of the single-frequency laser used as a light source. Another possibility would be the existence of surface layers, either as a layer of cupric oxide (CuO [14]) due to surface oxidation or as an exciton free dead layer [15].

In this paper, we therefore analyze the transmission spectrum of a thin plate of Cu_2O shown in Fig. 1, fully considering the coherence of the measuring laser beam by using the well-established coherence transfer matrix (CTM) [16] method to calculate the transmission spectra directly from the dielectric function (DF) of the crystal. We find that a single layer of Cu_2O without any exciton dead layer or other surface films is sufficient for a qualitative description, but a quantitative comparison at the level of accuracy of the experimental data requires a more complex structure with thin additional layers of a copper oxide, probably CuO or Cu_3O_2, which are known to exist on the surface of Cu_2O [17]. Furthermore, we consider the optical properties of the whole setup including reflection and scattering of the quartz windows of the cryostat and possible scattering from the optical surfaces of the sample. Also adjusting the strength of the indirect absorption process into the green exciton states, which is not so well known, it is possible to achieve excellent agreement between experiment and theory.

II. TRANSFER MATRIX CALCULATION OF THE TRANSMISSION SPECTRUM

In deriving the dielectric response of the excitons from the transmission spectrum by the CTM method, which is our final goal, we face the serious problem that, despite the long coherence length of the probe laser, we did not observe interference effects in the experimentally measured spectrum (see Fig. 1). The reason why no interference effects are observed may be twofold. On the one hand, the sample may show a slight wedge. Here, it turns out that already a small wedge of the order of $w = 1\ \mu$m/mm is enough to completely remove any interference effect by incoherently averaging the transmission over the finite laser spot size(fullwidthathalfmaximum = 170 μm). The other possibility would be a certain surface roughness, which also reduces the interference effects (see, e.g., Ref. [18]). In the following analysis, we include both effects. Therefore, we describe the light propagation through the sample by the coherent transfer and propagation matrices method (CTM), whereby the transfer matrices are modified due to interface scattering [18]

$$\mathbf{H}_{ij} = \frac{1}{\gamma\tau_{ij}}\begin{pmatrix}\gamma^2\tau_{12}\tau_{21} + \alpha\beta\rho_{21}^2 & \beta\rho_{ij}\\ \alpha\rho_{ij} & 1\end{pmatrix}. \tag{3}$$

The reflection and transmission coefficients for perpendicular incidence are given by

$$\tau_{ij} = \frac{2\tilde{n}_i}{\tilde{n}_i + \tilde{n}_j}, \quad \rho_{ij} = \frac{\tilde{n}_i - \tilde{n}_j}{\tilde{n}_i + \tilde{n}_j}, \tag{4}$$

and the roughness parameters are defined as

$$\alpha = \exp\left[-2\left(\frac{2\pi s_{ij} n_i}{\lambda}\right)^2\right], \quad \beta = \exp\left[-2\left(\frac{2\pi s_{ij} n_j}{\lambda}\right)^2\right],$$
$$\gamma = \exp\left[-\frac{1}{2}\left(\frac{2\pi s_{ij}}{\lambda}\right)^2 (n_j - n_i)^2\right], \tag{5}$$

with a surface or interface roughness of root mean square deviation s_{ij}. Note that already a roughness of the order of $\lambda/10$ reduces the coherence effects significantly.

The propagation matrix is

$$\mathbf{L}_j = \begin{pmatrix} e^{-i\beta_j} & 0\\ 0 & e^{i\beta_j}\end{pmatrix}, \quad \beta_j = \frac{2\pi}{\lambda_0}(n_j - i\kappa_j)d_j, \tag{6}$$

with d_j the thickness and $\tilde{n}_j = n_j - i\kappa_j$ the complex index of refraction of layer j.

For a single plate of Cu_2O, the system matrix would be (with 1 denoting the outside vacuum and 2 the sample)

$$\mathbf{S} = \mathbf{H}_{12}\mathbf{L}_2\mathbf{H}_{21}. \tag{7}$$

The reflection and transmission coefficients are obtained as

$$\rho = \frac{S_{12}}{S_{22}}, \quad \tau = \frac{1}{S_{22}}, \tag{8}$$

from which we obtain the reflectivity R and transmission T by taking the modulus square, as the medium on both sides is vacuum. These expressions can be easily extended to more complicated layer structures.

Since the diameter of the probe beam is finite, we must average over the thickness variation across the probe beam. Assuming a Gaussian intensity distribution $\propto \exp(-\rho^2/2\sigma_L^2)$ and a wedge w, we have a thickness distribution $\propto \exp(-\rho^2/2\sigma_d^2)$ with $\sigma_d = w\,\sigma_L$. The effects of the six cryostat windows can be considered by normalizing the transmission by the reflection and scattering losses $[(1 - R_Q(\lambda)][1 - S_Q(\lambda)]^{12}$, where $R_Q(\lambda)$ and $S_Q(\lambda)$ are the reflection and scattering of a single surface (note that, due to the window thickness of several millimeters, we can neglect the coherence of the light beam here).

To obtain the optical parameters of the P excitons like oscillator strength, linewidth, and resonance energies, we have to calculate the full DF $\varepsilon(\omega) = \varepsilon_r(\omega) + i\varepsilon_i(\omega)$ from which the complex index of refraction

$$\tilde{n} = n - i\kappa, \tag{9}$$

with $\kappa \geqslant 0$ can be calculated as

$$\begin{aligned} n(\omega) &= \sqrt{\tfrac{1}{2}[\varepsilon_r(\omega) + \sqrt{\varepsilon_r(\omega)^2 + \varepsilon_i(\omega)^2}]}, \\ \kappa(\omega) &= \sqrt{\tfrac{1}{2}[-\varepsilon_r(\omega) + \sqrt{\varepsilon_r(\omega)^2 + \varepsilon_i(\omega)^2}]}, \\ \alpha(\omega) &= \frac{2\omega}{c_0}\kappa(\omega), \end{aligned} \tag{10}$$

the last line giving the absorption coefficient. The real and imaginary part of the DF are related by a Kramers-Kronig transformation:

$$\begin{aligned} \varepsilon_r(\omega) &= n_b^2(\omega) + \frac{1}{\pi}\wp\int_{-\infty}^{\infty}\frac{1}{\omega' - \omega}\varepsilon_i(\omega)d\omega, \\ \varepsilon_i(\omega) &= -\frac{1}{\pi}\wp\int_{-\infty}^{\infty}\frac{1}{\omega' - \omega}\varepsilon_r(\omega)d\omega. \end{aligned} \tag{11}$$

From Eq. (10), it is clear that we need the expression for the DF that includes all excitonic resonances, i.e., the indirect processes involving the various phonons (see Ref. [11]), the P absorption lines, the corresponding continuum (see Refs. [3,19]), and also a background due to the higher excitonic transitions, for which we take the refractive index $n_b(\omega)$ given in Ref. [20].

The treatment of the indirect absorption processes that contribute to the background absorption requires great care, as there are several constraints on the positions of the exciton states (from absorption measurements) and the possible phonon modes (from symmetry [11] and resonance Raman studies [21]) that must be considered.

It has been known for a long time that the lowest energy transition is due to the Γ_3^- phonon (energy 13.5 meV) sideband of the $1S$ yellow ortho exciton [22–24], which recently has been reanalyzed, revealing a strong wave vector dependence of the deformation potential [11]. Its contribution to the imaginary part of the DF is given by [11]

$$\begin{aligned} \varepsilon_{i,\mathrm{ind},\Gamma_3^-}(\hbar\omega) = a_{\mathrm{ind},\Gamma_3^-}\sqrt{\hbar\omega - E_{1Sy,\Gamma_3^-}} \\ \times[1 + b_{,1Sy\Gamma_3^-}(\hbar\omega - E_{i1Sy,\Gamma_3^-})]^2\Phi(\hbar\omega - E_{1Sy,\Gamma_3^-}), \end{aligned} \tag{12}$$

where $E_{1Sy,\Gamma_3^-} = (2.04622 \pm 1 \times 10^{-5})$ eV is the threshold energy [9], and $a_{\mathrm{ind},\Gamma_3^-}$ is a parameter that must be adjusted by matching the absorption coefficient at energies near the onset to the empirical law Eq. (2). It turns out to be $a_{\mathrm{ind},\Gamma_3^-} = (7.20663 \pm 0.23) \times 10^{-6}/\mu\mathrm{eV}^{1/2}$. The parameter b_{1Sy,Γ_3^-} describes the nonlinearity due to a wave-vector-dependent deformation potential of the phonon mode η and has been determined to be 0.91×10^{-3}/meV [11]. Besides the indirect absorption process involving the Γ_5^- phonon (energy 10.8 meV, strength $\approx 3\%$ of the Γ_3^- process [10]), the only other important absorption process is due to the longitudinal optical phonon (symmetry Γ_4^-) with energy 82.1 meV. Its strength is not so well known and varies between 1% [10] to 20% [11] of $a_{\mathrm{ind},\Gamma_3^-}$. Therefore, we consider these strengths as fitting parameters in the following.

The next strong absorption band is due to the green exciton series with the lowest $1S$ ortho state at 2154.4 meV [25]. Here, we expect the Γ_3^- phonon to be strongest. In Ref. [11], the strength parameter is given as 2.4 times that of the $1S$ yellow state. Its nonlinearity parameter is 2.8×10^{-3}/meV [11]. All other green states are outside the considered spectral region. However, we must consider that the yellow S states with quantum numbers $n = 2$, 3, and 4 are strongly mixed with the green $1S$ state [26]; so they should contribute to the absorption according to their green content of 11% and 4%, respectively. Since for $n = 3$ and 4 the absorption threshold is above the yellow band edge energy ($E_{gy} = 2172.087$meV), only the $2S$ state must be considered below the gap. Since both the $1S$ green and the $2S$ yellow absorption strength is not well known, we consider them as fitting parameters as well.

However, there is another complication connected with these indirect processes, namely, that the exciton states are considerably broadened due to their short lifetime. The lifetime broadening can be easily derived from the recent second harmonic spectroscopy [25] to be 0.44 meV for the $1S$ green ortho state and 0.40 meV for the $2S$ yellow ortho state. For the $1S$ yellow ortho state, this effect can be neglected (width $\approx 2\,\mu$eV as determined from the transmission spectrum in Fig. 1). The contribution in the broadened case is given by

$$\begin{aligned} \varepsilon_{i,\eta}(\hbar\omega) = \frac{a_\eta}{\pi}(-1)^{1/4}\left\{\sqrt{\gamma_{i\eta} - i(\hbar\omega - E_\eta)}\arctan\left[\frac{\sqrt{iE_0}}{\sqrt{\gamma_\eta - i(\hbar\omega - E_\eta)}}\right] - \sqrt{\gamma_\eta + i(\hbar\omega - E_\eta)}\arctan h\left[\frac{\sqrt{iE_0}}{\sqrt{\gamma_\eta + i(\hbar\omega - E_\eta)}}\right]\right\} \\ + \frac{b_\eta}{2\pi}\left\{2\sqrt{E_0}\gamma_\eta + (-1)^{1/4}\sqrt{\gamma_\eta - i(\hbar\omega - E_\eta)}[i\gamma_\eta + (\hbar\omega - E_\eta)]\arctan\left[\frac{\sqrt{iE_0}}{\sqrt{\gamma_\eta - i(\hbar\omega - E_\eta)}}\right]\right. \end{aligned}$$

$$+(-1)^{1/4}[\gamma_\eta + i(\hbar\omega - E_\eta)]^{3/2} \arctan\left[\frac{i\sqrt{iE_0}}{\sqrt{\gamma_\eta + i(\hbar\omega - E_\eta)}}\right]\Bigg\}$$
$$+ \frac{b_\eta^2}{3\pi}\Bigg\{2\sqrt{E_0}\gamma_\eta[E_0 + 6(\hbar\omega - E_\eta)] - 3(-1)^{1/4}[\gamma_\eta - i(\hbar\omega - E_\eta)]^{5/2} \arctan\left[\frac{\sqrt{iE_0}}{\sqrt{\gamma_\eta - i(\hbar\omega - E_\eta)}}\right]$$
$$- 3(-1)^{3/4}[\gamma_\eta + i(\hbar\omega - E_\eta)]^{5/2} \arctan\left[\frac{i\sqrt{iE_0}}{\sqrt{\gamma_\eta + i(\hbar\omega - E_\eta)}}\right]\Bigg\}, \tag{13}$$

where E_η, γ_η, and $a_\eta = A_\eta a_{\text{ind}}$ denote the absorption threshold, the damping of the exciton state, and the strength of the indirect process η, respectively. Here, E_0 is a cutoff energy (for which we assume $E_0 = 2.5$ eV), and b_η denotes the nonlinearity.

The real part of the DF can in principle be obtained by a Kramers-Kronig transform, which for a contribution of the form of Eq. (12) is given by (here, $E_{g,i}$ denotes the threshold energy of the phonon process)

$$\varepsilon_{r,\text{ind}}(\hbar\omega) = a_{\text{ind}}\begin{cases} -\frac{2}{\pi}\left[\sqrt{E_0 - E_{g,i}} - \sqrt{E_{g,i} - \hbar\omega}\arctan\left(\sqrt{\frac{E_0 - E_{g,i}}{E_{g,i} - \hbar\omega}}\right)\right] & \text{for } \hbar\omega < E_{g,i} \\ -\frac{2}{\pi}\left[\sqrt{E_0 - E_{g,i}} - \sqrt{\hbar\omega - E_{g,i}}\text{atanh}\left(\sqrt{\frac{\hbar\omega - E_{g,i}}{E_0 - E_{g,i}}}\right)\right] & \text{for } \hbar\omega > E_{g,i} \end{cases}$$
$$+ \frac{a_{\text{ind}} b_\eta}{3\pi}\begin{cases} 2\sqrt{E_0 - E_{g,i}}(E_0 - 4E_{g,i} + 3\hbar\omega) + 6(E_{g,i} - \hbar\omega)^{3/2}\text{atan}\left[\sqrt{\frac{E_0 - E_{g,i}}{E_{g,i} - \omega}}\right] & \text{for } \hbar\omega < E_{g,i} \\ 2\sqrt{E_0 - E_{g,i}}(E_0 - 4E_{g,i} + 3\hbar\omega) + 3(\hbar\omega - E_{g,i})^{3/2}\ln\left[\frac{\sqrt{\frac{E_0 - E_{g,i}}{\hbar\omega - E_{g,i}}} - 1}{\sqrt{\frac{E_0 - E_{g,i}}{\hbar\omega - E_{g,i}}} + 1}\right] & \text{for } \hbar\omega > E_{g,i} \end{cases}. \tag{14}$$

For the broadened expression, there exists no closed solution, so we must do it numerically. However, it turns out that the difference to the nonbroadened results in Eq. (14) is negligible compared with the dominant contributions due to the background dielectric constant.

All the parameters used in the analysis are given in Table I.

From semiconductor optics [13,19,27], we get the following expression for the contribution of the P absorption lines to the imaginary part of the DF

$$\varepsilon_{i,P}(\omega) = \sum_{n=2}^{\infty} \tilde{f}_n \frac{1}{\pi}\frac{\Gamma_n + 2A_n(\omega - \omega_n)}{(\omega - \omega_n)^2 + \Gamma_n^2}. \tag{15}$$

Here, the sum goes over the P states, and $\tilde{f}_n$ denotes strength constants proportional to the oscillator strengths per volume [27] ($f_n/V = 2m_0\varepsilon_0/\pi e_0^2\hbar^2 \cdot \tilde{f}_n$), ω_n, Γ_n, andA_n are the

TABLE I. Values of general parameters used in the fit of the transmission spectrum.

Parameter	Notation	Value	Note	Parameter	Notation	Value	Note
Thickness	D_{Cu_2O} (μm)	32.11	Fit	Indirect transitions	a_{ind} (μeV$^{-1/2}$)	7.20663×10^{-6}	Ref. [11]
Wedge	w ($\frac{\mu m}{mm}$)	1	Fit	$1Sy(5+) - \Gamma_3^-$	A	1.000	Ref. [11]
					E_{1Sy,Γ_3^-}(meV)	2046.228	Ref. [9]
					β (1/meV)	0.91×10^{-3}	Ref. [11]
					γ_{1Sy,Γ_3^-} (μeV)	2	Fit
Roughness	s_{rhg}(nm)	25.0	Fit	$2Sy(5+) - \Gamma_3^-$	A	1.313	Fit
					E_{2Sy,Γ_3^-}(meV)	2152.60	Ref. [33]
					γ_{2Sy,Γ_3^-} (meV)	0.40	Ref. [33]
					β (1/meV)	2.0×10^{-3}	Ref. [33]
Band gap shift	Δ (μeV)	-178.6	Fit	$1Sy(5^+) - \Gamma_{42}^-$	A	0.188	Fit
					$E_{1Sy,\Gamma_4^-(2)}$(meV)	2114.83	Ref. [11]
					γ_{1Sy,Γ_3^-} (μeV)	2	Fit
Strength	a_c	1.645×10^{-3}	Fit	$1Sg(5^+) - \Gamma_3^-$	A	2.470	Fit
					$E_{1Sg(5+),\Gamma_3^-}$(meV)	2167.7	Ref. [33]
					β (1/meV)	2.0×10^{-3}	Fit
					γ_{2Sy,Γ_3^-} (meV)	0.44	Ref. [33]
Urbach-tail 1	E_{ur1} (μeV)	98.0	Fit	$1Sg(5^+) - \Gamma_5^-$	A	0.975	Fit
					$E_{1Sg(5+),\Gamma_5^-}$	2165.5	Ref. [33]
Urbach-tail 2	E_{ur2} (μeV)	3442	Fit	$1Sy(5^+) - \Gamma_5^-$	A	0.115	Fit
					$E_{1Sy(5+),\Gamma_5^-}$(meV)	2143.53	Ref. [9]
					γ_{1Sy,Γ_3^-} (μeV)	2	Fit
Fraction	a_{ur}	0.90	Fit				

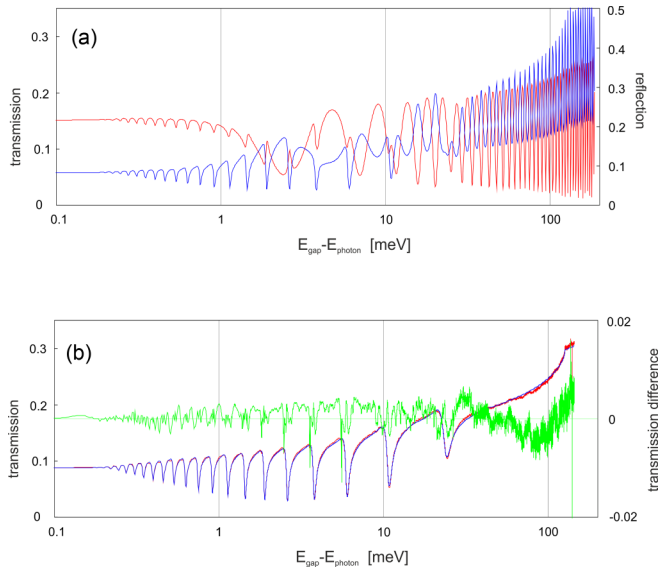

FIG. 2. (a) Reflection (red) and transmission (blue) spectra of a plate of Cu_2O with a constant thickness of 30 μm, calculated with the coherent transfer matrix (CTM) method. (b) Comparison of the measured transmission spectrum (red line) with the calculated spectrum assuming a single layer of Cu_2O (with parameters given in Tables I and II) The green line gives the difference of the spectra. Note the logarithmic energy scale.

resonance energy, damping, and asymmetry of an exciton state, which are to be determined. Furthermore, m_0, e_0, and ε_0 denote the electron mass, charge, and the permittivity of the vacuum, respectively. Both the damping Γ_n and the asymmetry parameter A_n, which in principle are energy dependent, will be assumed to be constant. However, there arises the problem that, far away from the resonance, the contribution of each P state to ε_i decreases only proportional to $1/(\omega-\omega_n)$, which leads to a negative overall DF above the band edge, resulting in a peak in the transmission spectrum directly above the band edge in contrast to experiment [see Fig. 2(b)]. One can correct for this discrepancy by introducing either a frequency dependence of A_n that sets $A_n = 0$ above a certain distance from the resonance as proposed in Ref. [6] or by an energy-dependent broadening that goes over into an Urbach-like tail, as proposed in Ref. [28]. Here, we achieve this by multiplying the damping with a function $g_n(\omega) = \cosh[(\omega-\omega_n)/3\Gamma_n]$, whereby the factor 3 has been chosen to obtain the best agreement with the experimental line shape. The contribution of the P lines to the real part of the DF is given by

$$\varepsilon_{r,P} = \sum_n \tilde{f}_n \frac{1}{\pi} \frac{(\omega-\omega_n) - 2\Gamma_n A_n}{(\omega-\omega_n)^2 + \Gamma_n^2}, \tag{16}$$

as calculated by the Kramers-Kronig transformation of Eq. (15), but disregarding the factor $g_n(\omega)$ [29].

For the P continuum absorption, we have from Ref. [30]

$$\varepsilon_{i,c}(\hbar\omega) = a_c \left(1 + \frac{\hbar\omega - E_g}{\mathrm{Ry}}\right) \Phi(\hbar\omega - E_g), \tag{17}$$

where E_g is the yellow band gap, and Ry is the exciton Rydberg energy.

TABLE II. Results for the parameters of the Rydberg exciton states as obtained from the fits of the transmission spectrum according to the dielectric theory. The errors for the energies and linewidths are $\sim \pm 1\mu$eV, while that for the oscillator strengths and asymmetry parameters are $\sim \pm 1\%$, except otherwise indicated.

Quantum number n =	Energy $E_n(\mu\mathrm{eV})$	Oscillator strength $\tilde{f}_n(\mu\mathrm{eV})$	Linewidth $\Gamma_n(\mu\mathrm{eV})$	Asymmetry A_n
2	$-23\,677 \pm 5$	15.268	1280 ± 5	-0.488
3	$-10\,720 \pm 5$	8.554	305.2 ± 2	-0.277
4	-5986 ± 2	5.043	150.8	-0.225
5	-3780.4	2.7136	81.83	-0.254
6	-2594.1	1.5568	45.87	-0.261
7	-1887.8	0.9507	30.99	-0.272
8	-1436.6	0.6532	22.88	-0.260
9	-1127.6	0.4491	17.63	-0.246
10	-908.1	0.3208	14.16	-0.237
11	-747.1	0.2388	12.10	-0.239
12	-625.2	0.1803	10.53	-0.263
13	-530.7	0.1403	9.63	-0.250
14	-455.9	0.1096	8.55	-0.227
15	-395.9	0.0903	8.06	-0.223
16	-346.2	0.0656	6.96	-0.249
17	-306.0	0.0495	6.58	-0.216
18	-272.2	0.0338	6.04	-0.202
19	-243.6	0.0244	6.20	-0.181
20	-219.9	0.0181	7.15	-0.075
21	-199.5	0.0082	6.50	0.05
22	-182.7	$(1 \pm 0.3) \times 10^{-3}$	5 ± 1	0.0 ± 0.1

The corresponding real part is then

$$\varepsilon_{r,c}(\hbar\omega) = \frac{a_c}{\pi} \begin{cases} \frac{E_0-E_g}{\mathrm{Ry}} - \left(1 + \frac{\hbar\omega-E_g}{\mathrm{Ry}}\right) \ln\left(\frac{E_g-\hbar\omega}{E_0-\hbar\omega}\right) & \text{for } \hbar\omega < E_g \\ \frac{E_0-E_g}{\mathrm{Ry}} - \left(1 + \frac{\hbar\omega-E_g}{\mathrm{Ry}}\right) \ln\left(\frac{\hbar\omega-E_g}{E_0-\hbar\omega}\right) & \text{for } \hbar\omega > E_g \end{cases}. \tag{18}$$

We also must treat the Urbach tail for a complete description [11]. Assuming the following form,

$$\varepsilon_{iUT}(\hbar\omega) = a_c \exp\left(\frac{-E_g + \hbar\omega}{E_u}\right) \Phi(E_g - \hbar\omega), \tag{19}$$

we obtain for the real part

$$\varepsilon_{r,UT}(\hbar\omega) = \frac{a_c}{\pi} \begin{cases} \exp\left(\frac{-E_g+\hbar\omega}{E_u}\right) \mathrm{Ei}\left(\frac{E_g-\hbar\omega}{E_u}\right) & \text{for } \hbar\omega < E_g \\ \exp\left(\frac{-E_g+\hbar\omega}{E_u}\right) \Gamma\left(0, \frac{\hbar\omega-E_g}{E_u}\right) & \text{for } \hbar\omega > E_g \end{cases}, \tag{20}$$

where $\mathrm{Ei}(z)$ denotes the exponential integral and $\Gamma(a, z)$ the incomplete Gamma function [31].

In total, we get for the imaginary part of the DF

$$\varepsilon_i(\omega) = \sum \varepsilon_{i,\mathrm{ind}}(\omega) + \varepsilon_{i,c}(\omega) + \varepsilon_{i,UF}(\omega) + \varepsilon_{i,P}(\omega), \tag{21}$$

and for the real part

$$\varepsilon_r(\omega) = \sum \varepsilon_{r,\mathrm{ind}}(\omega) + \varepsilon_{r,c}(\omega) + \varepsilon_{r,UF}(\omega) + \varepsilon_{r,P}(\omega). \tag{22}$$

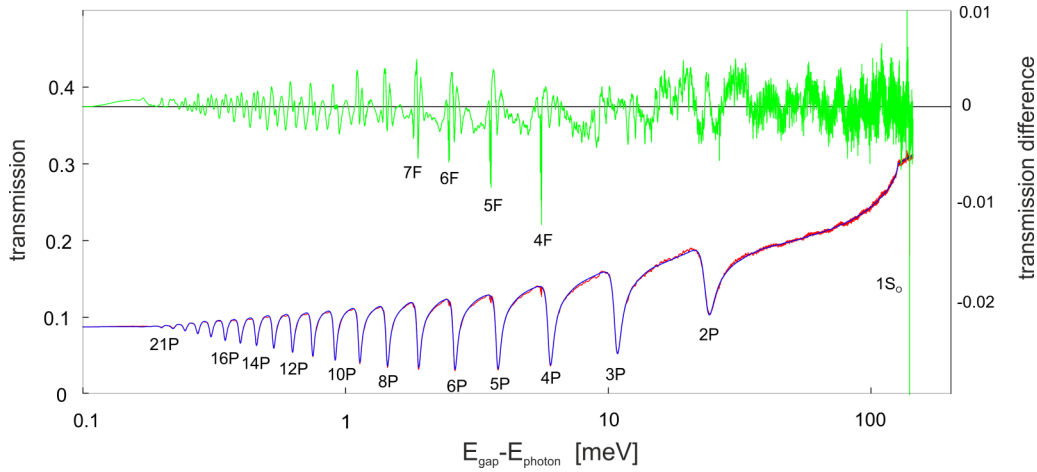

FIG. 3. Comparison of the measured transmission spectrum (red line) with the calculated spectrum assuming a layered structure of a plate of Cu2O with thin layers of CuO on top and bottom (thickness, other parameters see text), the green line gives the difference of the spectra. Note the logarithmic energy scale.

From the DF, we calculate with Eqs. (8) and (10) the transmission spectrum $T(\omega) = |\tau(\omega)|^2$. The relevant parameters, which include the resonance energies, strength parameters, dampings, and asymmetries of all P excitons, are obtained by searching for the best fit of the calculated spectrum to the experimental data. In this way, impacts of spectral changes of the reflectivity of the sample, which were neglected in the previous analyses [1,2,11] but amount up to 10% of the effect, are consistently considered.

To determine the global parameters s_{Cu_2O}, d_{Cu_2O}, and w, we adjusted the value of the calculated transmission in the spectral region below the indirect absorption threshold E_{1Sy,Γ_3^-}, where the absorption due to the exciton states should be zero, to the measured one and fitted the transmission in the spectral region close to the threshold to Eq. (12).

In Fig. 2(a), the result of the calculation of the reflection and transmission for a sample with constant thickness is plotted, showing pronounced interference fringes. As demonstrated in part (b), these interference effects are completely absent in a slightly wedged sample ($w = 1\mu$m/mm). The comparison with the measured transmission spectrum [red curve in Fig. 2(b)] shows that a single layer of Cu_2O can reproduce the whole transmission spectrum from the quadrupole yellow 1S line to the yellow band edge at least qualitatively with sufficient accuracy. However, in the spectral region below the 2P transition, there is a systematic deviation between the experimental and theoretical transmission spectrum, which looks like a very broad oscillatory behavior with period ~150 meV. Considering Fabry-Perot resonances as the potential origin of these oscillations, this would correspond to a thin layer with optical thickness of only 2 μm. Because such a thin plate is not present in the setup, one must consider other origins of this structure. Here, one might think of a very thin layer of CuO or Cu_3O_2 [17] on the sample, which might occur due to oxidation or a thin layer due to polishing. Indeed, considering such a layer (with index of refraction given by $n_{CuO}(\lambda)^2 = 4.05 + 2.4\lambda^2/[\lambda^2 - (0.447\,\mu\text{m})^2]$ [32], an absorption constant $\kappa_{CuO} = 2.09 \times 10^{-3}$, and a thickness $d_{CuO} = 0.64$ μm), we obtain the transmission spectrum shown in Fig. 3 that completely eliminates this oscillations.

In comparison of Fig. 2(b) (and Fig. 3) with Fig. 1, we clearly see that we must fully consider the coherence properties of the laser to describe the transmission spectrum across the whole range from the yellow 1S ortho exciton to the yellow band gap correctly. The residual differences of the order of a few percent [green curve in Fig. 2(b)] will be discussed below.

III. DISCUSSION

The foregoing analysis has shown that a fully consistent description of the transmission spectrum is possible using the correct DF and the CTM method.

A closer look at the residual differences [green curve in Fig. 2(b)] reveals that there are four types of deviations behaving quite differently:

(1) Most prominent are the sharp peaks slightly above the P exciton lines for $n = 4$ to 8, which are triplets. These are the well-known F exciton lines [33], which have not been included in the DF.

(2) Above the band gap, the transmission of the sample is expected to be smooth, as only continuous processes (indirect phonon-assisted processes and absorption into the continuum) occur. We observe a pronounced oscillatory pattern shown in Fig. 4(a) (red line). The oscillation consists of several components with oscillation periods from 100 to 500 eV. If the origin were Fabry-Perot resonances of various quartz plates, their thicknesses would be between 1.7 and 8 mm, corresponding roughly to the thicknesses of the optical windows. Then we expect these interferences to occur in the whole spectral range with similar periods. Indeed, around the indirect absorption edge, similar structures do exist [see Fig. 4(a), blue line].

(3) Looking more closely to the fit around the P lines [see also Fig. 4(b)], we see a characteristic deviation that looks like a second derivative of the P line shape. This points toward a deficiency of the asymmetric Lorentz line shape, Eq. (15), that requires a more accurate theory of the phonon-assisted processes. Note that, until now, all efforts to quantitatively derive the line shapes of the P excitons from the basic interaction processes [13] have not been successful (see, e.g., Ref. [34]).

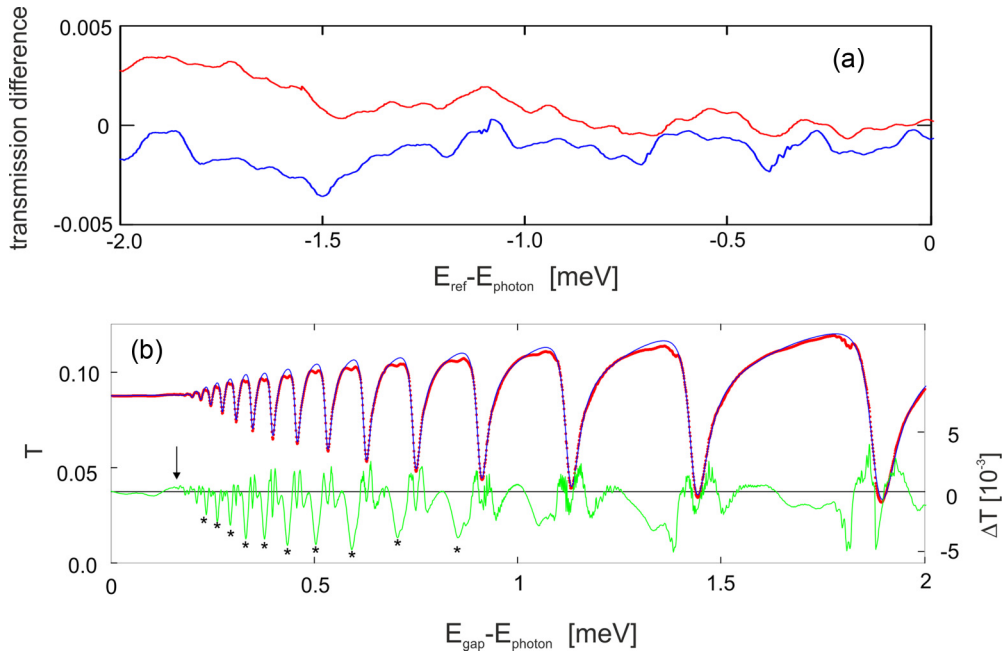

FIG. 4. (a) Comparison of residual transmission spectra directly above the band gap (red curve, $E_{\rm ref} = E_g$) with that 100 meV below the band gap (blue curve, $E_{\rm ref} = E_g - 100$ meV) showing a similar structure. (b) Transmission spectrum (red experiment, blue calculation) near the band gap showing Rydberg transitions up to $n = 22$. The green colored line gives the difference of measured and calculated spectra showing additional absorption peaks (marked by *) and weak residual interferences, which are continuing above the band gap (arrow).

(4) Most interesting is the residual transmission spectrum just below the band gap in the region of the Rydberg states [see Fig. 3(b)]. By properly fitting the asymmetric Lorentzian lines of the P states, the weak peaks situated between the P lines (marked by *) already observed previously [35] turn out to be much stronger than the interference structure that continues from above the band edge. As the energy difference to the next lower P state scales as $1/n^3$, one might speculate that these lines originate in forbidden transitions into D exciton states, which are shifted from the P states by a different quantum defect [36] and become allowed through the electric field of the charged impurities [6]. To substantiate this hypothesis, a thorough analysis of these lines in different samples including the effects of external electric fields is underway.

The parameters of the fit can be grouped into three categories: (1) the parameters of the P lines (resonance energies, oscillator strength, linewidth, and asymmetry), (2) the parameters of the continuum absorption (band gap shift, absorption strength, and Urbach tail) and of the phonon-assisted indirect transitions, and (3) the parameters describing the sample properties (thickness, wedge, and surface roughness). The first two sets of parameters are given in Table I, while those of the P lines are given in Table II and shown in Fig. 5.

Defining a hypothetical "exact" energy of each P state in the form of a modified quantum defect formula [37]

$$E_n = -\frac{\mathrm{Ry}}{(n-\delta_n)^2} + E_g \quad \text{with} \quad \delta_n = \delta_0 + \frac{\delta_2}{(n-\delta_0)^2} + \frac{\delta_4}{(n-\delta_0)^4} + \frac{\delta_6}{(n-\delta_0)^6} + \ldots, \tag{23}$$

the parameters of the best fit are given in Table III. Equation (23) allows us to describe all P lines in the range between $n = 2$ and 22 with an accuracy of $\pm 1\ \mu$eV [see Fig. 5(a)]. For the oscillator strengths and linewidths, we used a similar quantum defect formula as for the energies

$$f_n = f_0 \frac{(n-\delta_{fn})^2 - 1}{(n-\delta_{fn})^5} \quad \text{with} \quad \delta_{fn} = \delta_{f0} + \frac{\delta_{f2}}{(n-\delta_{f0})^2} + \frac{\delta_{f4}}{(n-\delta_{f0})^4} + \frac{\delta_{f6}}{(n-\delta_{f0})^6} + \ldots. \tag{24}$$

For the linewidth we assume

$$\Gamma_n = \Gamma_0 \frac{(n-\delta_{\Gamma n})^2 - 1}{(n-\delta_{\Gamma n})^5} + \Gamma_r \quad \text{with} \quad \delta_{\Gamma n} = \delta_{\Gamma 0} + \frac{\delta_{\Gamma 2}}{(n-\delta_{\Gamma 0})^2} + \frac{\delta_{\Gamma 4}}{(n-\delta_{\Gamma 0})^4} + \frac{\delta_{\Gamma 6}}{(n-\delta_{\Gamma 0})^6} + \ldots, \tag{25}$$

where Γ_r is a sample-dependent homogeneous broadening constant. For the obtained parameters, see Table III.

The resonance energies of the P excitons and the linewidths can be described with Eq. (23) or Eq. (25) by a generalized quantum defect formula for all quantum numbers from $n = 2$ to 22 with good accuracy [see inset in Fig. 4(a)]. The same holds for the linewidths. In contrast, the oscillator strength follows a quantum defect equation only up to $n = 15$; for

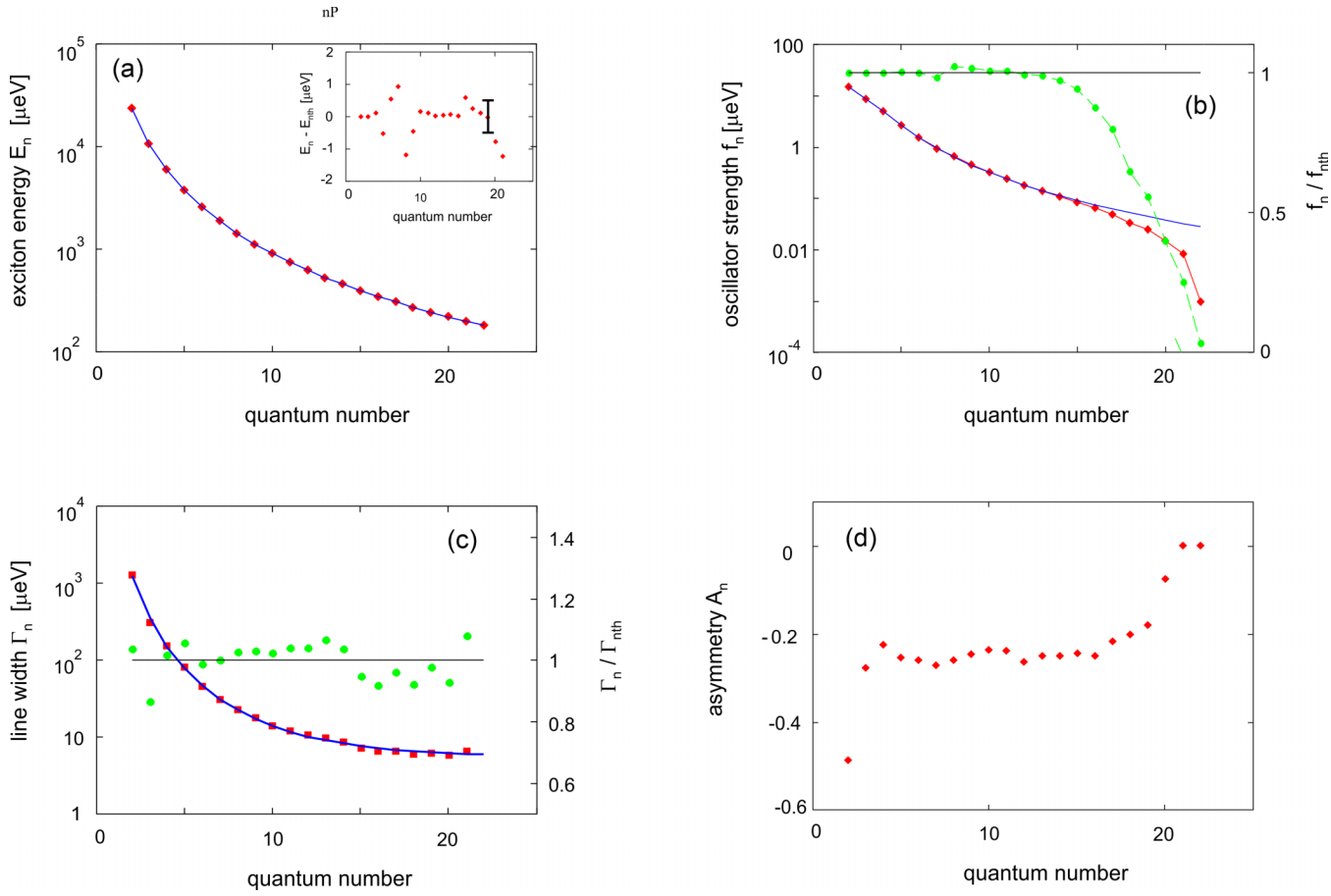

FIG. 5. (a) Energies, (b) oscillator strengths, (c) linewidths, and (d) asymmetry parameters for the Rydberg P exciton states are plotted against the principal quantum number n. The red diamonds give the experimental values (see Table II), the full blue lines the fitted expressions Eqs. (23)–(25) for diagrams (a)–(c), respectively. The inset in (a) gives the difference of the fitted energies to Eq. (23). The vertical bar gives the approximate error. The green dots in (b) and (c) give the ratio of the quantities from the fits to that obtained from Eqs. (24) and (25), showing that the experimental values are reproduced only up to $n = 15$ for the oscillator strength but up to $n = 22$ for the linewidth. Note that, for the asymmetry parameter, no theoretical expression exists.

higher n, the effects of charged impurities must be considered [6].

Finally, we discuss the problem of the number of absorbed photons that are converted into elementary excitations in the crystal. Usually, this is calculated from the Bouguer-Lambert law as [3]

$$\dot{N}_{\text{phot}} = [1 - \exp(-\alpha d)](1 - R_{Cu_2O})I_0. \tag{26}$$

This, however, is not possible anymore, as one has standing waves due to interference inside the crystal and scattering due to surface roughness leading to a loss of laser intensity. Instead, one must calculate the absorbed power per volume of the crystal applying Fermi's golden rule. This leads to the following expression:

$$\frac{dP}{dtdV} = 2\frac{\omega}{n^2}\langle u\rangle\kappa, \tag{27}$$

where $\langle u\rangle$ is the energy density of the electromagnetic field

$$\langle u\rangle = \tfrac{1}{2}\varepsilon_0 n^2 |E|^2, \tag{28}$$

TABLE III. Parameters for the Rydberg exciton states according to Eqs. (23)–(25).

Parameter	Energy	Parameter	Oscillator strength	Parameter	Linewidth
Ry (meV)	−87 461.98	$f_0(\mu\text{eV})$	285.42	Γ_0 (μeV)	8360
δ_0	−0.206	δ_{f0}	0.3931	$\delta_{\Gamma 0}$	0.112
δ_2	0.135	δ_{f2}	−0.8870	$\delta_{\Gamma 2}$	−0.21
δ_4	7.709	δ_{f4}	41.67	$\delta_{\Gamma 4}$	0
δ_6	−25.957	δ_{f6}	−86.23	$\delta_{\Gamma 6}$	0
E_g(meV)	21 720.701			$\Gamma_r(\mu\text{eV})$	4.23

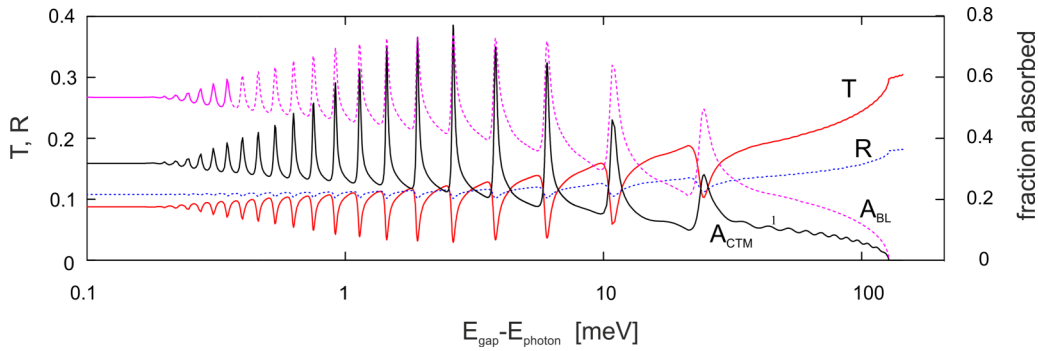

FIG. 6. Transmission (T, red line) and reflection (R, blue dotted line) spectra (left ordinate) in comparison with the spectrum of the absorbed fraction of laser power incident on the sample using the simple Bouguer-Lambert law (A_{BL}, magenta dashed line, right ordinate) and the exact calculation in the CTM method (A_{CTM}, black line, right ordinate).

where n and κ are the real and imaginary part of the refractive index [see Eq. (6)]. Here, we have assumed that $\kappa \ll n$. The field inside the sample is given by

$$E(z) = E_r \exp\left(\frac{i\beta z}{d}\right) + E_l \exp\left[-\frac{i\beta(d-z)}{d}\right], \tag{29}$$

where β is given by Eq. (6). Here, E_r and E_l are the electric field strengths of the right and left propagating waves at the surface of the sample at $z = 0$ and can be obtained from the transmission [Eq. (8)] by

$$\begin{pmatrix} E_l \\ E_r \end{pmatrix} = \mathbf{L}_1 \mathbf{H}_{12} \begin{pmatrix} 0 \\ \tau \end{pmatrix}. \tag{30}$$

This shows that the laser intensity inside the sample might considerably vary spatially over distances of <100 nm.

To obtain the total absorbed power inside the sample, one must integrate over the sample thickness (note that this also requires averaging over the sample surface because of the wedge). This gives

$$\frac{dP}{dt} = \left[1 - \exp\left(-\frac{2\omega\kappa d}{c_0}\right)\right]\eta_{\mathrm{cor}} I_0. \tag{31}$$

Here, η_{cor} is given by

$$\eta_{\mathrm{cor}} = |E_r|^2 + |E_l|^2 \exp\left(\frac{2\omega\kappa d}{c_0}\right) + 2\mathrm{Re}\{E_r \bar{E}_l \times \exp\left[\frac{i\omega(n - i\kappa)d}{c_0}\right]\}. \tag{32}$$

As seen from Fig. 6 , where the results of Eqs. (26) and (31) are compared, using the Bouguer-Lambert law overestimates the absorbed power by almost a factor of 2. This must be considered not only in deriving the densities of excitons or electron-hole pairs (see Ref. [3]) after optical excitation but also in the recently published theory of optical nonlinearities of Rydberg excitons if the excitation laser has a long coherence length [38]. Also, a calculation of the absorbance A by the relation $A + R + T = 1$ does give wrong results (see the corresponding curves in Fig. 6), as the sample shows substantial surface scattering.

IV. CONCLUSIONS

In this paper, we have analyzed the transmission spectrum of a thin plate of Cu_2O in the range of the absorption of the yellow exciton states with the CTM method and demonstrated that a consistent quantitative description is possible. The analysis gives accurate values for the parameters of the Rydberg P excitons such as resonance energies, oscillator strengths, and linewidths. These can be parameterized by a generalized quantum defect formula. Fortunately, it turns out that the more exact CTM method almost gives the same results for the parameters of the P excitons as the usually used simpler analysis based on the Bouguer-Lambert law, at least for high quantum numbers $n > 10$ (see Ref. [1]). However, if one needs a highly accurate quantitative analysis, e.g., in the investigations of the action of an electron-hole plasma on the Rydberg states, the CTM method, as exemplified in this paper, should be used.

ACKNOWLEDGMENTS

We thank Wolf-Dietrich Kraeft, University of Rostock, Germany; Holger Fehske, University of Greifswald, Germany; and Peter Grünwald, Aarhus University, Denmark, for helpful discussions. D.S. thanks the Deutsche Forschungsgemeinschaft for financial support (Project No. SE 2885/1-1). The Dortmund side acknowledges the support by the Deutsche Forschungsgemeinschaft through the International Collaborative Research Centre TRR160 (Project A8, Grant No. 249492093) and AS 459/3-1 (Grant No. 386069213).

[1] T. Kazimierczuk, D. Fröhlich, S. Scheel, H. Stolz, and M. Bayer, Nature **514**, 343 (2014).

[2] M. Aßmann and M. Bayer, Adv. Quantum Techn. **3**, 1900134 (2020).

[3] J. Heckötter, M. Freitag, D. Fröhlich, M. Aßmann, M. Bayer, P. Grünwald, F. Schöne, D. Semkat, H. Stolz, and S. Scheel, Phys. Rev. Lett. **121**, 097401 (2018).

[4] D. Semkat, H. Fehske, and H. Stolz, Phys. Rev. B **100**, 155204 (2019).

[5] S. O. Krüger, H. Stolz, and S. Scheel, Phys. Rev. B **101**, 235204 (2020).

[6] D. Semkat, H. Fehske, and H. Stolz, Eur. Phys. J. Spec. Top. **230**, 947 (2021).

[7] J. H. Lambert, *Photometria, Sive de Mensura et Gradibus Luminis, Colorum et Umbrae, Sumptibus Vidae Eberhardi Klett* (Bibliothèques de l'Université de Strasbourg, Augsburg, 1760), https://docnum.unistra.fr/digital/collection/coll12/id/13932/rec/1.

[8] Wikipedia, Beer-Lambert law, https://en.wikipedia.org/wiki/Beer%E2%80%93Lambert_law.

[9] J. Brandt, D. Fröhlich, C. Sandfort, M. Bayer, H. Stolz, and N. Naka, Phys. Rev. Lett. **99**, 217403 (2007).

[10] K. E. O'Hara, *Relaxation Kinetics of Excitons in Cuprous Oxide*, Thesis, University of Illinois, Urbana-Champaign, 1999.

[11] F. Schöne, H. Stolz, and N. Naka, Phys. Rev. B **96**, 115207 (2017).

[12] Note that the usual text book derivation of Eq. (2) going back to Elliott [16] is wrong, as we have shown in Ref. [11], and that Eq. (2) results only if one assumes a q-dependent exciton-phonon interaction and only for small enough excess energies. For higher photon energies, it must be replaced by Eq. (12).

[13] Y. Toyozawa, J. Phys. Chem. Solids **25**, 59 (1964).

[14] H. Wieder and A. W. Czanderna, J. Phys. Chem. **66**, 816 (1962).

[15] C. Klingshirn, *Semiconductor Optics*, 4th ed. (Springer, Heidelberg, Berlin, New York, 2012).

[16] M. Klein and Th. Furtac, *Optics* (John Wiley & Sons, New York, 1986).

[17] D. E. Mencer, M. A. Hossain, R. Schennach, T. Grady, H. McWhinney, J. A. G. Gomes, M. Kesmez, J. R. Parga, T. L. Barr, and D. L. Cocke, Vacuum **77**, 27 (2004).

[18] C. L. Mitsas and D. I. Siapkas, Appl. Opt. **34**, 1678 (1995).

[19] H. Haug and S. W. Koch, *Quantum Theory of Optical and Electronic Properties of Semiconductors* (World Scientific, Singapore, 2004).

[20] T. Ito, T. Kawashima, H. Yamaguchi, T. Masumi, and S. Adachi, J. Phys. Soc. Jpn. **67**, 2125 (1998).

[21] P. Y. Yu and Y. R. Shen, Phys. Rev. B **12**, 1377 (1975).

[22] E. F. Gross, J. Phys, Chem. Solids **8**, 172 (1959).

[23] E. F. Gross, Sov. Phys. Uspekhi **5**, 195 (1962).

[24] S. Nikitine, in *Optical Properties of Solids*, edited by S. Nudelman and S. S. Mitra (Plenum, New York, 1969).

[25] A. Farenbruch, D. Fröhlich, D. R. Yakovlev, and M. Bayer, Phys. Rev. Lett. **125**, 207402 (2020).

[26] F. Schweiner, J. Main, G. Wunner, and Chr. Uihlein, Phys. Rev. B **95**, 195201 (2017).

[27] H. Stolz, F. Schöne, and D. Semkat, New J. Phys. **20**, 023019 (2018).

[28] L. Bányai and S. W. Koch, Z. Phys. B **63**, 283 (1986).

[29] For $g_n(\omega)$ included in Eq. (15), no analytical Kramers-Kronig transform has been found, but a numerical Kramers-Kronig transform of Eq. (15) with $g_n(\omega)$ included does show no significant deviations from Eq. (16).

[30] R. J. Elliott, Phys. Rev. **108**, 1384 (1957).

[31] M. Abramowitz and I. A. Stegun (Eds.), *Handbook of Mathematical Functions with Formulas, Graphs, and Mathematical Tables*, National Bureau of Standards, Applied Mathematics Series 55 (U.S. Government Printing Office, Washington D.C., 1964).

[32] P. Johansson, Phys. Rev. B **83**, 195408 (2011).

[33] J. Thewes, J. Heckötter, T. Kazimierczuk, M. Aßmann, D. Fröhlich, M. Bayer, M. A. Semina, and M. M. Glazov, Phys. Rev. Lett. **115**, 027402 (2015).

[34] F. Schweiner, J. Main, and G. Wunner, Phys. Rev. B **93**, 085203 (2016).

[35] P. Grünwald, M. Aßmann, J. Heckötter, D. Fröhlich, M. Bayer, H. Stolz, and S. Scheel, Phys. Rev. Lett. **117**, 133003 (2016).

[36] F. Schöne, S. O. Krüger, P. Grünwald, H. Stolz, S. Scheel, M. Aßmann, J. Heckötter, J. Thewes, D. Fröhlich, and M. Bayer, Phys. Rev. B **93**, 075203 (2016).

[37] T. F. Gallagher, *Rydberg Atoms, Cambridge Monographs on Atomic Physics* (Cambridge University Press, Cambridge, 2005).

[38] V. Walther and Th. Pohl, Phys. Rev. Lett. **125**, 097401 (2020).